Experimental identification of whirl flutter characteristics in a small-scale rotor rig

A. Tatar, D. Rezgui, B. Titurus
University of Bristol, Department of Aerospace Engineering,
Queens Building, University Walk, Bristol, BS8 1TR, UK

Abstract
This paper presents the development of a small-scale unpowered experimental test rig with a bladed rotor along with its dynamic model. The novel attributes of this work are: (1) the use of a compact portable vertical wind tunnel and with the pendulum-like accelerometer-instrumented rotor rig, (2) assessment of the in-operation vibrations and whirling dynamics for future use in the large scale experiments, and (3) analysis of the rig-specific rotor dynamics phenomena. This work experimentally and numerically studies the proposed rotor rig with the main emphasis on its modal characteristics. Owing to its design characteristics, it is shown analytically and experimentally, that the rig features four dominant lateral backward and forward whirling vibration modes in relatively wide frequency range during its windmilling operation. Consequently, it is determined that the rotor rig represents a useful simplified low order system suitable for studies of a range or dynamic phenomena such as transient resonance crossing, whirl flutter and geometric nonlinearity effects.

1 Introduction

Whirl flutter is an aeroelastic instability condition, which affects a broad range of bladed rotors supported on elastically deformable foundations. Whirl flutter occurs due to the coupling between aerodynamic and gyroscopic moments acting on the propeller-rotor when the support stiffness or damping between the propeller-rotor and nacelle are relatively low [1], [2]. Whirl flutter can limit the performance of propeller configurations in fixed-wing and tilt-rotor aircrafts. So far, good progress has been achieved in understanding the physics behind it such as backward whirling mode instability [1]–[3].

In rotorcraft aeromechanics, two dynamic models which are known as Reed's [1] and Johnson's [4] model are widely used to understand the physics behind the whirl flutter phenomenon. The so-called Reed's model has 2 degrees of freedom (DOF), describing the pitching and yawing motions of the rotor. It basically represents a bladed-rotor system on the elastic support. The more advanced Johnson's model has 9 DOF, which include rotor-blade, pylon and wing dynamics. For tiltrotors, proprotors, turboprops and propellers, numerous linear and nonlinear analyses have been conducted to investigate whirl flutter and its boundaries [3], [5]. Rotors are designed to avoid any possible whirl flutter effects within their operational boundaries [6]–[9]. By the 2000's, aeromechanics of tiltrotors have become an important research topic due to its complex nature. Consequently, new tiltrotor test rigs have been developed to investigate their aeroelastic behaviour in wind tunnels in recent years [10]–[16]. Further whirl flutter rig development and wind tunnel test activities have been carried out for propellers [17], [18]. Selected rigs designed for the whirl flutter tests in wind tunnels can be seen in Figure 1.

Modal parameter identification associated with the classical fixed-wing flutter instability has also attracted attention of many researchers over the years. In 2019, the online wing flutter monitoring studies were performed during wind tunnel testing and flight operations using operational modal analysis techniques [19]–[21]. However, more research is required to develop the online modal parameter identification for the whirl flutter problems and experiments. The development of an early warning whirl flutter detection system is the central theme of this study.

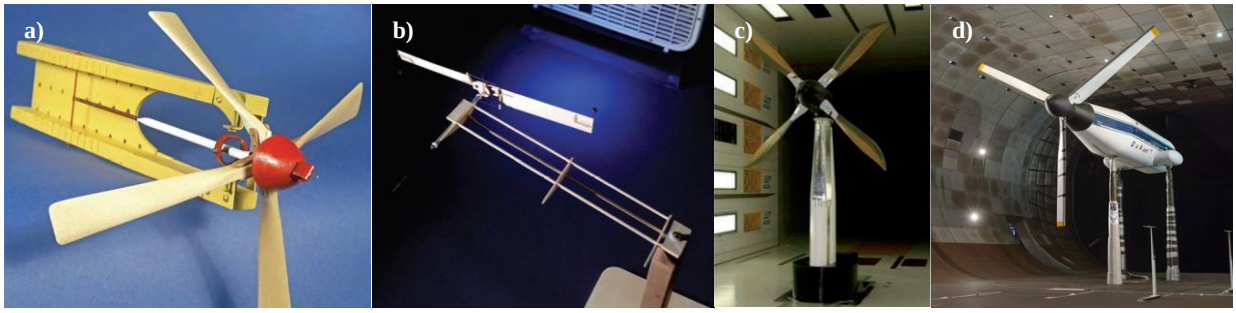

Figure 1: Selected whirl flutter test rigs: a) hinged blades propeller [22], b) small-scale tiltrotor [7], c) medium-scale tiltrotor [16], d) large-scale tiltrotor [11]

This paper provides an update on the vibration identification and monitoring research of potentially catastrophic rotor dynamics phenomena in the framework of the UK-funded EPSRC MENtOR (Methods and Experiments for Novel Rotorcraft) project. This project intends to develop knowledge and modelling tools for future energy efficient reconfigurable multi-rotor aerospace vehicles with focus on their improved vibration and aeroelastic stability characteristics. The main aim of this paper is to describe the development of the small-scale unpowered (wind milling) whirl flutter test rig and to present the numerical and experimental dynamics characterization of this rig when operated in a vertical wind tunnel. For this purpose, a 3D dynamic model of the whirl flutter test rig is developed using the finite element method by incorporating gravity and gyroscopic forces. In the non-rotating case, experimental and numerical modal analyses are carried out to identify the modal behaviour. Similarly, the vibration responses of the test rig during operation are investigated in the vertical wind tunnel under varying air stream speed conditions. To identify the modal parameters of the whirl flutter test rig, a vibration monitoring algorithm is proposed, where peak-finding and logarithmic decrement methods are used.

2 Development of rotor test rig

A new whirl flutter test rig named the Bristol Whirling Rotor Rig (BWRR) is motivated by the classical 2 DOF Reed's model and its well-known experimental realization [1]. At the same time, the presented design takes into consideration the requisite compact nature of the rig and its simple architecture. Figure 2 shows the CAD model and manufactured assembly of the BWRR, respectively.

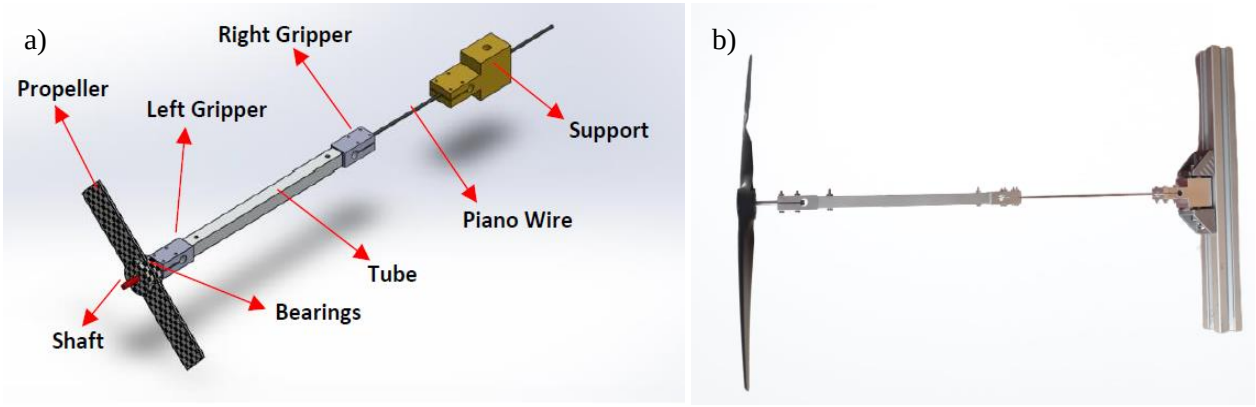

Figure 2: Bristol Whirling Rotor Rig (BWRR), a) CAD model, b) manufactured assembly

The key design feature of the rig is its pendulum-like configuration where the gravity loads help to longitudinally stabilise the rig, which is otherwise very soft in its transversal (bending) direction. This feature enables the dynamics of interest to exist within the limited speed range of the vertical wind tunnel. Another important design feature of the rig is the intended separation between the sources of inertial and

restoring loads. This division promotes the dominance of a small number of vibration modes in the desired frequency range as well as ability to adjust the rig's modal frequencies through either inertia or stiffness-driven modifications.

The BWRR consists of a propeller, two bearings, a steel shaft, an aluminium tube, two aluminium grippers, a steel piano wire and an aluminium supporting element, respectively, as seen in Figure 2a. The two-bladed propeller of diameter 279 mm and pitch of 102 mm is made of a fibre-glass composite. It is supported on the non-rotating shaft via two ball bearings. The shaft is connected to the left gripper. The left and right grippers are connected to an aluminium tube via bolted connections. The tube allows placement of the accelerometers for vibration monitoring. These parts are connected to the support through the 1 mm diameter piano wire. The length of the wire can be changed leading to the adjustable support stiffness. This design feature enables significant alterations in the rig's dynamic behaviour. The propeller-rotor system is expected to present the whirling dynamics in the small vertical wind tunnel. Important geometry and material properties of the BWRR are presented in Table 1.

Table 1: Selected parameters of the BWRR

Parameter	Propeller	Shaft	Tube	Left Gripper	Right Gripper	Wire
Length [m]		0.05	0.15	0.05	0.05	0.2
Outer diameter [m]	0.279	0.04				0.001
Inner diameter [m]	0.00635	0.02				
Thickness [m]	0.002		0.001			
Mass [kg]	0.0261	0.0045	0.0145	0.0140	0.0147	0.0012
Material density [kg/m^3]		7800	2700	2700		7800
Young's modulus [GPa]		210	70	70		210
Shear modulus [GPa]		80	27	27		80

The BWRR is sized to be used in the small-scale vertical wind tunnel where the propeller can rotate freely under the controlled free stream air flow. The vertical wind tunnel consists of the fan segment, collector and working sections as shown in Figure 3a. The fan segment, located at the bottom of the wind tunnel, houses the 3×3 grid of off-the-shelf fans which produce the required air flow. The collector section accelerates the air flow to the working section where it can reach a velocity of up to 2.5 m/s. The working section has a length of 600 mm and a cross section of 340 mm × 340 mm, which can conveniently accommodate the main working part of the BWRR, as seen in Figure 3b.

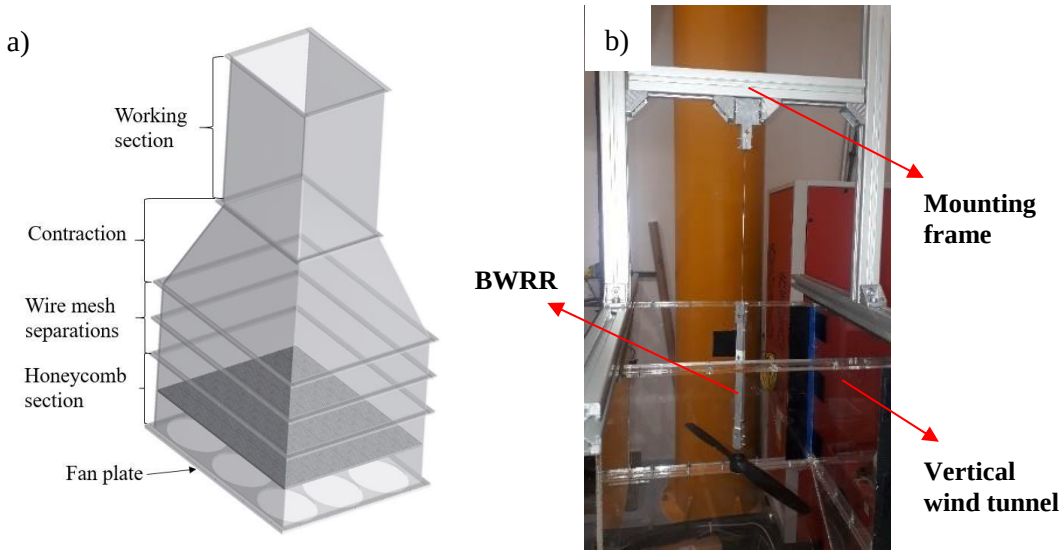

Figure 3: Vertical wind tunnel, a) CAD model, b) test configuration with BWRR

3 Methods

3.1 Numerical modelling

A dynamic model for the BWRR was developed using the finite element method (FEM). The beam elements where each node has 6 DOFs; including lateral, torsional and axial motions; are used. The components of the BWRR, namely the shaft, grippers, tube, piano wire, are modelled with Timoshenko beam elements [23]. The propeller is assumed to be rigid while the bearing-holding shaft is flexible. The model is fixed at the support. The main characteristics of the dynamic model is that the finite element formulation incorporates gyroscopic forces, gravity and potentially other axial forces induced during its operation. The stiffening effect due to gravity forces in the axial direction of the rotor rig is considered in the Timoshenko beam formulation [23]. For creating the final model, 85 nodes in total are used by taking into account locations of the key parts of the assembled rig. Each beam element is around 0.005 m long.

To maintain initial focus on the rotor dynamics behaviour, the model without aerodynamic forces is formed and studied first. Consequently, this study effectively evaluates the in-vacuo properties caused by the gyroscopic effects and gravity. The system's equations of motion can be written in the following form

$$\mathbf{M}\ddot{\boldsymbol{q}}(t) + [\mathbf{C} + \mathbf{G}]\dot{\boldsymbol{q}}(t) + \mathbf{K}\boldsymbol{q}(t) = 0 \tag{1}$$

where $\mathbf{M}$, $\mathbf{C}$, $\mathbf{G}$, $\mathbf{K}$ are system mass, damping, gyroscopic and stiffness matrices, respectively. Here, $\boldsymbol{q}$ represents the nodal coordinates with axial, torsional and lateral displacements. After defining the system equation of motion in Eq.1, the state space representation of the dynamic model can be written as

$$\begin{Bmatrix} \dot{\boldsymbol{q}} \\ \ddot{\boldsymbol{q}} \end{Bmatrix} = \begin{bmatrix} \mathbf{0} & \boldsymbol{I} \\ -\mathbf{M}^{-1}\mathbf{K} & -\mathbf{M}^{-1}[\mathbf{C} + \mathbf{G}] \end{bmatrix} \begin{Bmatrix} \boldsymbol{q} \\ \dot{\boldsymbol{q}} \end{Bmatrix}. \tag{2}$$

By defining $\boldsymbol{x}^T = \{\boldsymbol{q}, \dot{\boldsymbol{q}}\}$, Eq.2 can be written in the compact state space form

$$\{\dot{\boldsymbol{x}}\}_{2n\times 1} = [\mathbf{A}]_{2n\times 2n}\{\boldsymbol{x}\}_{2n\times 1} \tag{3}$$

where $\boldsymbol{x}$ is known as the state vector and $\mathbf{A}$ is the state space system matrix.

The natural frequencies and mode shapes of the problem in Eq.1 are calculated by solving the standard eigenvalue problem arising from Eq.3. This model and various types of analyses, including eigenvalue analysis, are completed in MATLAB 2019a software environment.

3.2 Experimental modal parameter identification

Modal parameters such as natural frequencies, mode shapes, modal damping can be obtained using Experimental Modal Analysis (EMA) and Operational Modal Analysis (OMA) [24]. In this section, the use of these two methods to provide relevant experimental information is provided.

EMA is employed to provide baseline information about the underlaying dynamics of the rig with non-rotating rotor. The resulting information supports model-experiment correlation effort and provides the starting point for the following in-operation experimental activities. An OMA approach is chosen to observe the changes in the selected modal properties during the rig operation triggered in response to the imposed air flow conditions.

During both experimental stages, EMA and OMA, the same test infrastructure was used. The data acquisition was completed using National Instruments NI-9234 4-Channel Dynamic Signal Acquisition Module in one (OMA with single accelerometer) or two channel (EMA in SISO configuration) configurations. The dynamic response of the rig was measured using one single-axis accelerometer PCB Piezotronics 352A24. The data acquisition was managed and controlled by an in-house software utilizing Data Acquisition Toolbox of MATLAB 2019a. The sampling frequency was 2048 Hz during all experiments whilst the length of acquired signal varied depending on the specifics of individual experiments.

3.2.1 Experimental modal analysis setup

In EMA, an impact excitation and output accelerations are both measured so that the appropriate Frequency Response Function (FRF) can be computed. Subsequently, the modal parameters are estimated by fitting the FRFs. A basic experimental setup with an impact hammer and non-rotating rotor is shown in Figure 4. A PCB Piezotronics modally tuned impact hammer for small sized structures with a soft rubber tip and a single-axis ICP accelerometer were used to identify FRFs. The analysis was principally carried out to identify the natural frequencies of the BWRR. In this study, these quantities support the model-experiment correlation, experiment-driven dynamic rig tuning and provide the reference for the following in-operation OMA tests. In response to the dynamic tuning effort whilst aiming at sufficiently low global rig natural frequencies, the length of the steel piano wire was adjusted to 203 mm.

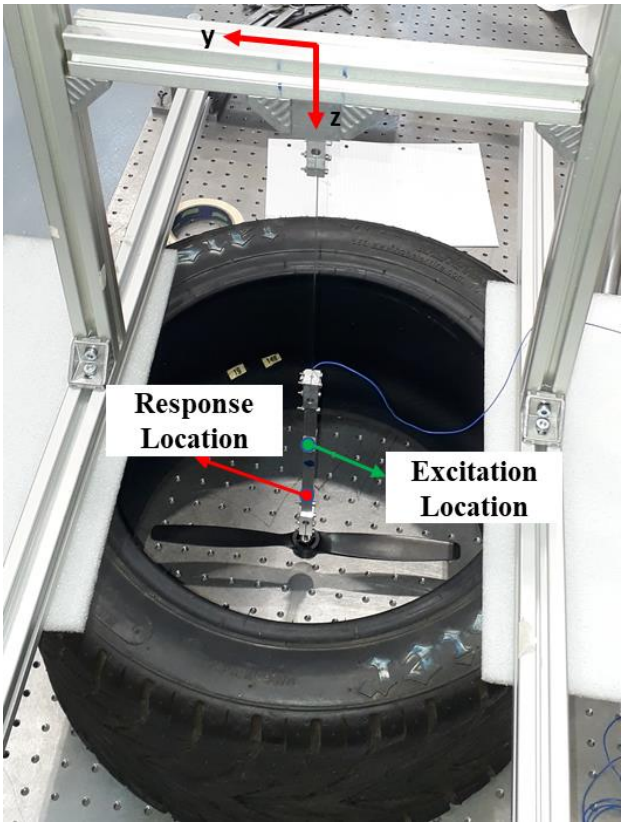

Figure 4: Experimental setup for impact hammer test

3.2.2 Operational modal analysis setup

An OMA test strategy is employed to determine the changes in the selected modal properties during test rig operation under the controlled flow conditions. Whilst only outputs are expected to be observed during a conventional OMA, the approach chosen here is to introduce the time-localized impulsive perturbations which are superimposed on the dynamic responses of the rig produced by the steady-state or slowly varying wind tunnel-induced rig operation.

The vibration behaviour of the BWRR is thus monitored by observing the manually triggered transient dynamics in the working wind tunnel. For this study, only one single-axis accelerometer is used to measure the output accelerations. A non-instrumented soft impact method was used to trigger the presence of the low modes of interest in the transient impulse response of the rig.

For identifying the in-operation modal parameters and future online monitoring, a suite of off-the-shelf and in-house developed MATLAB tools is employed according to the baseline architecture shown in Figure 5.

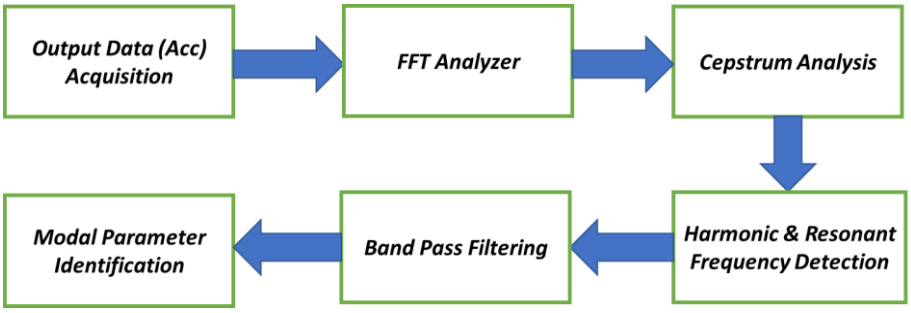

Figure 5: The proposed monitoring process flowchart

The monitoring starts with the measured raw accelerations. Then, these data are processed using the Fast Fourier Transform (FFT) and cepstrum analysis [25], respectively. The FFT reveals the key participating frequencies in the frequency range of interest, including both the resonant and harmonic content. The cepstral analysis determines the repeating patterns in the frequency domain related to the rotor harmonics or other effects. This step is performed to enable the observation and then separation of the steady harmonic and transient modal content. Next, bandpass filtering tools can be used to further pre-process the data for the focused identification of the excited backward and forward whirling frequencies. The obtained filtered data can be also used to engage other basic (e.g. the Logarithmic Decrement) or advanced (e.g. Least Square Complex Exponential method, Stochastic Subspace Identification) methods to identify the modal damping or mode shapes.

4 Results

4.1 Non-rotating modal behaviour

4.1.1 Experimental modal analysis

Figure 6 presents an example of the identified inertance FRF (acceleration/force) for the selected SISO configuration (see section 3.2.1). This FRF indicates the presence of lateral (bending) modes. Only the frequency range from 0 to 20 Hz is included to evidence the distribution of the key dynamic features. The presented FRF also indicates that there is a very good modal separation between the low frequency modes of interest and any subsequent higher order modes.

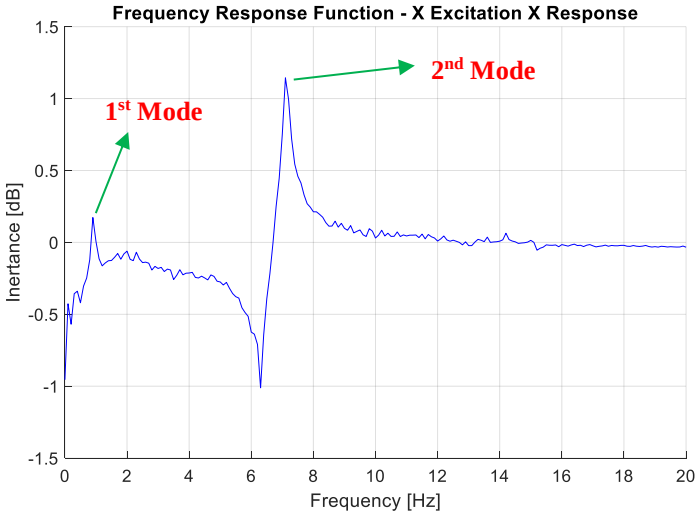

Figure 6: Frequency response function for lateral vibrations

As can be seen in Figure 6, there is also good modal separation between the two indicated modal peaks. The first bending mode is detected at 0.9 Hz and the second bending mode is present at 7.1 Hz for this non-rotating stationary case. It should be noted that the propeller was not locked and was able to move freely during the tests. As a result, small misalignment, free-play and other rotor hub joint imperfections were able to introduce spurious effects that effectively polluted the main modes of interest. Additionally, whilst the rig is nominally axisymmetric, the presence of only two-bladed rotor creates a noticeable inertial asymmetry. This small asymmetry manifests itself as a small modal separation between two pairs of theoretically multiple modes of an axisymmetric structure.

It can be concluded that, withing the wide frequency range, there are only four bending modes which are well separated from the higher modes. Additionally, these four modes come in two families or pairs where the first pair can be attributed to the first classical modal pattern (with only a single modal node matched with the clamping location) and the second modal pair linked with the second classical modal pattern (with one additional modal node located in the region of the aluminium tube). The modal separation within each observed modal family is small and caused by the lack of perfect inertial axial symmetry. However, the introduction of rotation will accentuate and increase this separation across the four modes.

4.1.2 Model-experiment correlation

The numerical modal analysis of the BWRR for an undamped non-rotating (stationary) case was carried out using the numerical modelling approach defined in section 3.1 and system parameters given Table 1. Normalized mode shapes are plotted for the first nine modes in Figure 7, where the corresponding natural frequencies are also shown.

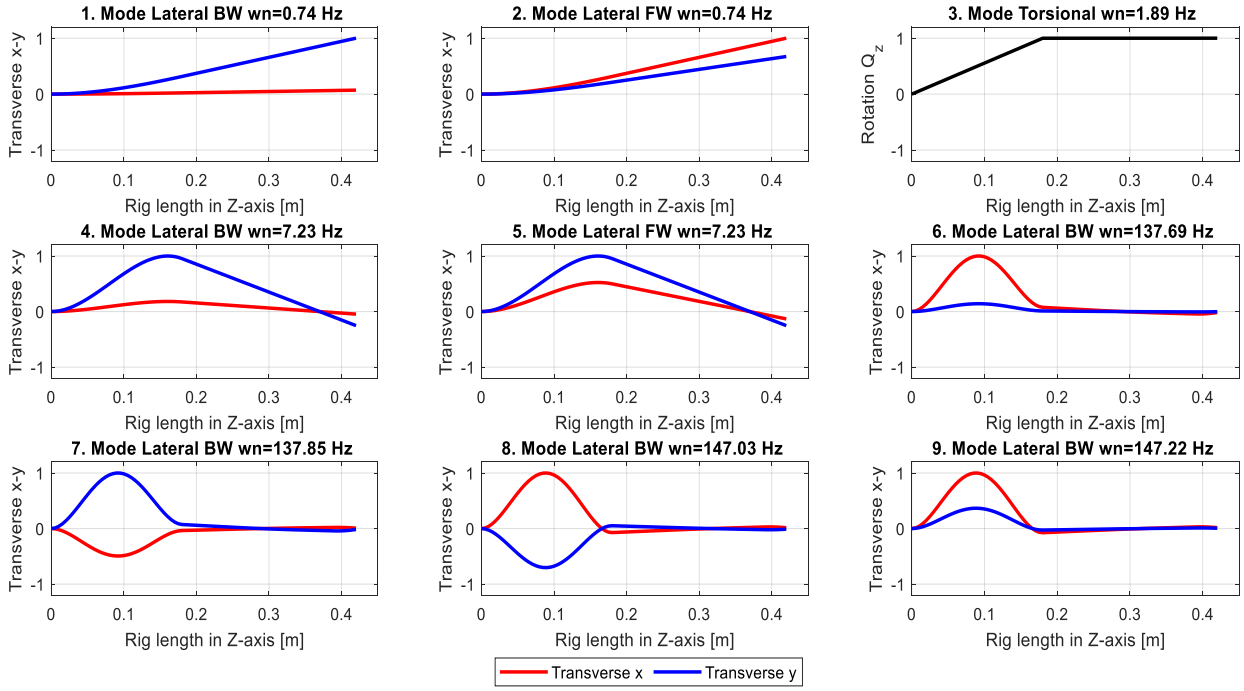

Figure 7: Numerically calculated mode shapes of the BWRR – non-rotating case

Inspecting Figure 7, there are 8 bending and 1 torsional mode among the first nine modes. Further, in agreement with the previous experimental observations, it can be seen that the first two pairs of bending modes, and previously not observed torsional mode at 1.89 Hz, are well separated from the rest of the modal spectrum. The next calculated mode families are present at 138 Hz and 147 Hz and they are significantly dominated by the piano wire activity.

Experimentally and numerically computed vibration modes are compared in Table 2, where the errors between the two sets of data are also shown. During EMA, the lateral modes which are numbered as modes 1, 2, 4 and 5 were captured successfully. However, modes 6, 7, 8 and 9 are not observed well because an accelerometer and impact locations on the tube cannot be used to detect (or excite) the associated modes properly. Furthermore, the mode 3 which is a torsional mode could not be captured since the instrumentation was not configured to observe this motion. The error in the second lateral mode family (modes 4 and 5) highlights the very good correlation. However, the error in the first lateral mode family (mode 1 and 2) are thought to be only satisfactory. It should be noted that the frequency correlation for the very low frequencies of the first mode family is comparatively more difficult to establish.

Table 2: Vibration modes of the BWRR in non-rotating (stationary) case

Mode #	Numerical Natural Freq. [Hz]	Experimental Natural Freq. [Hz]	Error %	Mode Type
1	0.74	0.90	17.6	Lateral
2	0.74	0.90	17.6	Lateral
3	1.89	--	--	Torsional
4	7.23	7.10	1.8	Lateral
5	7.23	7.10	1.8	Lateral
6	137.69	--	--	Lateral
7	137.85	--	--	Lateral
8	147.03	--	--	Lateral
9	147.22	--	--	Lateral

4.2 Rotating case modal behaviour

4.2.1 Vertical wind tunnel run-up vibration tests

The free-wheeling run-up vibration tests of the BWRR were carried out in the vertical wind tunnel by introducing the step change between the zero and maximum value of the air stream speed (corresponding to 13 Volts). In the unblocked vertical wind tunnel, the air stream speed with respect to the controlled operating fan voltage was measured with an anemometer and the resulting relationship is shown in Figure 8. Since the propeller cannot rotate freely, due to its own mechanical resistances, with the air stream produced by the voltage under 6 Volts, only the measured results from 6 to 13 Volts are given.

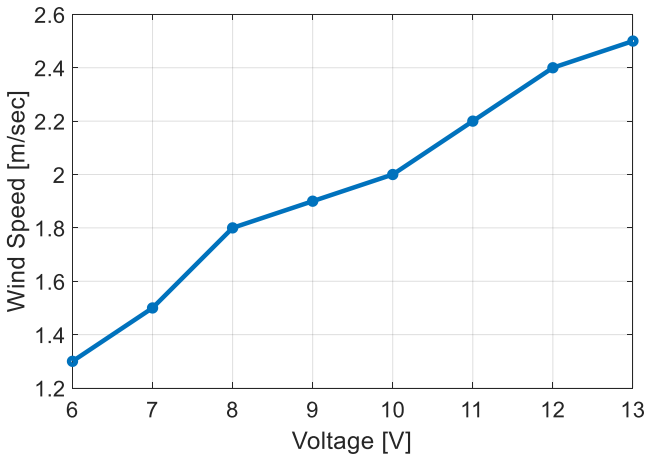

Figure 8: Air stream speed versus fan voltage

The outcome of this test is presented using the short-time FFT technique and the resulting spectrogram (waterfall diagram) is shown in Figure 9, for which "spectrogram" function in MATLAB 2019a is used. Here, the lateral (bending) backward and forward whirling modes, rotational frequencies and other features are clearly seen.

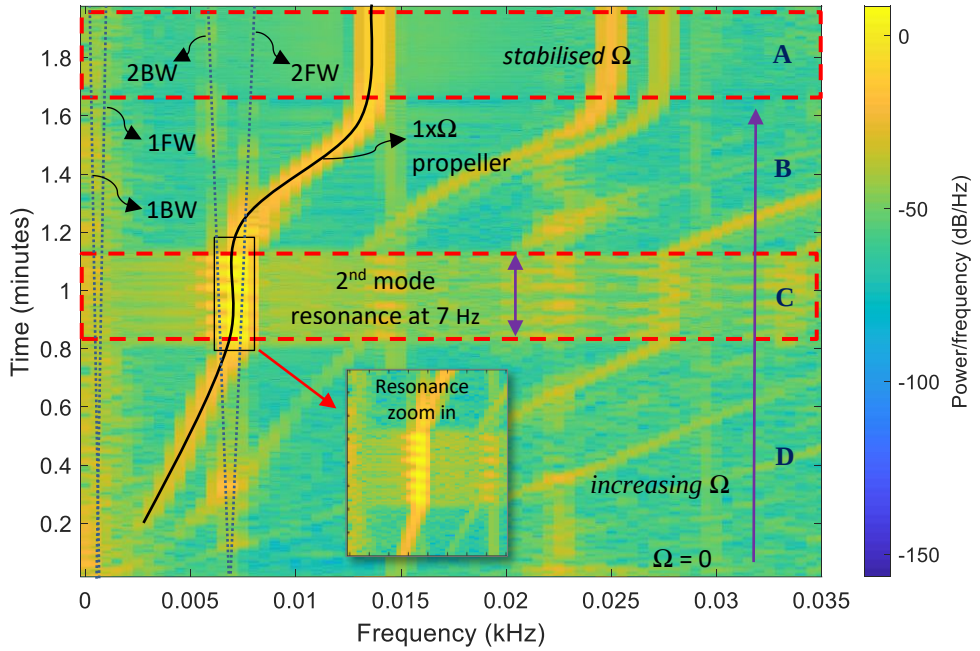

Figure 9: Free-wheeling BWRR run-up test response and its spectrogram

The spectrogram in Figure 9 is divided into 4 regions denoted as "A", "B", "C" and "D". Region B and D are identified as the run-up regions. Here, the propeller speed increases in response to the step-changed free stream velocity. Therefore, the harmonics related to the rotational frequency Ω can easily be tracked. First (1BW and 1FW) and second (2BW and 2FW) lateral mode families are also tracked. In this rotating system, forward (FW) lateral modes increases while backward (BW) lateral modes decreases with respect to the increasing propeller speed. In region C, the second lateral mode family (2^{nd} backward and forward lateral modes) at around 7 Hz, which was already detected during the impact hammer test, is excited due to its match with the rotor frequency. Therefore, the strong resonance and other broadband frequency effects are triggered and seen in this region. Region A is identified as the steady-state region since the propeller speed does not change with time. The propeller reaches its maximum speed which is identified as 824 rpm in this region. The sideband effects become also visible due to the rotating machinery features such as the bearing and blade imperfections. Overall, the harmonic and resonant responses can be clearly seen in the spectrogram where the rotational and blade passing frequencies are predominant. Therefore, these frequencies will be identified and filtered out for further whirling dynamics investigations.

4.2.2 Vertical wind tunnel steady-perturbation test

Impulse response tests in the vertical wind tunnel were done by tapping the stationary (no rotor rotation and air flow) and operating (induced rotor rotation due to applied air flow) BWRR in its steady-state conditions without recording the applied input force. In the case presented here, the propeller rotated at 824 rpm ≈ 13.73 Hz under 2.5 m/sec air stream velocity (produced by 13V) whilst being loaded by both aerodynamic and gyroscopic forces. Impulse responses in time domain for both non-rotating and rotating cases are plotted in Figure 10a. Time domain vibration responses clearly show that there is a free decay observed in the non-rotating case whereas vibration response in the rotating case is dominated by the steady-state vibration component produced a variety of the sources, e.g. unbalance and aerodynamic loads.

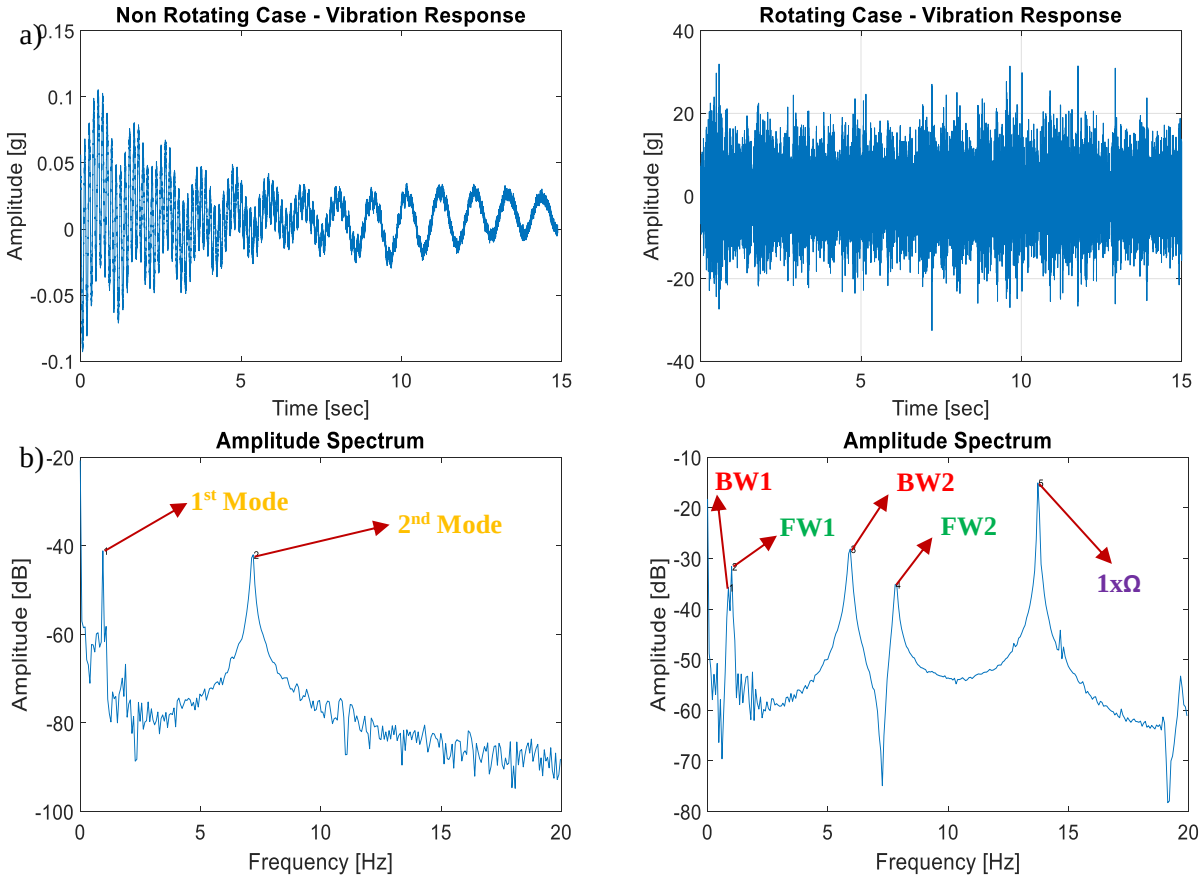

Figure 10: Impulse responses for non-rotating and rotating cases: a) time domain, b) frequency domain

Throughout the use of the vibration monitoring algorithm, the FFT analysis is used for resonance detection and the cepstrum analysis tool is used for the rotor harmonics detection as seen in Figure 10b and Figure 11a, respectively. Based on the significant peak values in the power cepstrum and amplitude spectrum, the harmonics and resonance frequencies can be detected with the simple peak-finding tools. FFTs of the acceleration impulse responses are plotted up to 20 Hz for both non-rotating (static) and rotating (under aerodynamic and gyroscopic forces) cases as seen in Figure 10b. For the non-rotating case, the first and second lateral modes were found to be at 0.94 Hz and 7.19 Hz, respectively. For the rotating case, the first (BW1) and second (BW2) lateral backward whirling modes were detected at 0.87 Hz and 5.93 Hz, respectively, whereas the first (FW1) and second (FW2) lateral forward whirling modes were detected at 1.00 Hz and 7.80 Hz, respectively.

During the monitoring process, band-pass filtering is used to isolate single-mode components for modal damping identification of the corresponding vibration mode from its impact-induced free decay response. For the band-pass filtering, “bandpass” function is employed from Signal Processing Toolbox of MATLAB 2019a, where a minimum-order filter with a stopband attenuation of 60 dB is used. After applying a band-pass filter for the specified narrow frequency band, the free vibration response of the 3rd whirling mode (BW2) at 5.93 Hz is plotted in Figure 11b. Under these conditions, natural frequencies and modal damping values are estimated with peak-finding and logarithmic decrement methods [26]. Modal parameter estimates for the first four lateral vibration modes and 13V wind tunnel input are presented in Table 3.

Table 3: Estimated modal parameters of the BWRR in the rotating case with 13V input

Modal Parameter	Mode 1 (BW1)	Mode 2 (FW1)	Mode 3 (BW2)	Mode 4 (FW2)
Natural Frequency [Hz]	0.87	1.00	5.93	7.80
Modal Damping	0.0256	0.0222	0.0108	0.0090

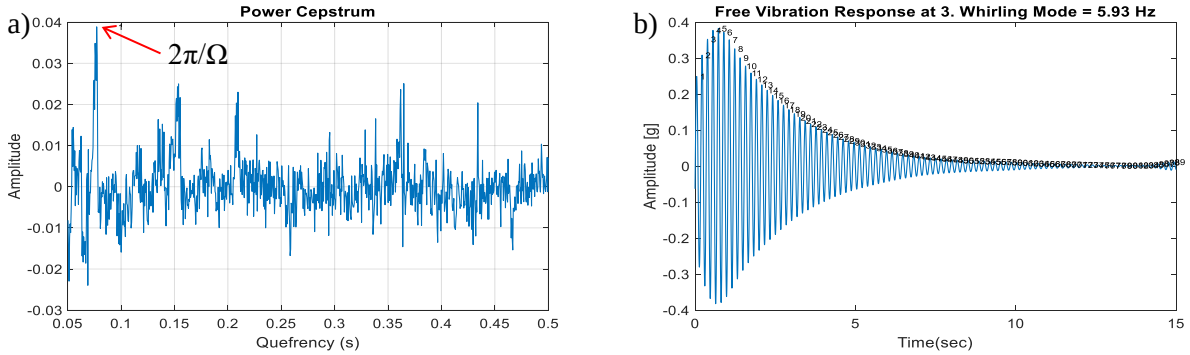

Figure 11: Vibration responses for 13V wind tunnel input: a) cepstrum analysis, b) BW2 band-pass filtered impulse response

For further illustration of the test strategy, two tests cases with and without impulse input in the working vertical wind tunnel are described next. These two tests were carried out under 790 rpm (13.17 Hz) rotor speed and 2.2 m/sec air stream velocity. The resulting spectrograms are plotted in Figure 12. Figure 12b clearly shows free decay responses at the second lateral backward (BW2) and forward whirling (FW2) modes. Interestingly, albeit weakly present, Figure 12a also features these two whirling modes even though no impulse was applied. These results suggest that conducting the natural frequency monitoring without any input is a plausible option that will be considered in future studies and in the large-scale rotor rig context.

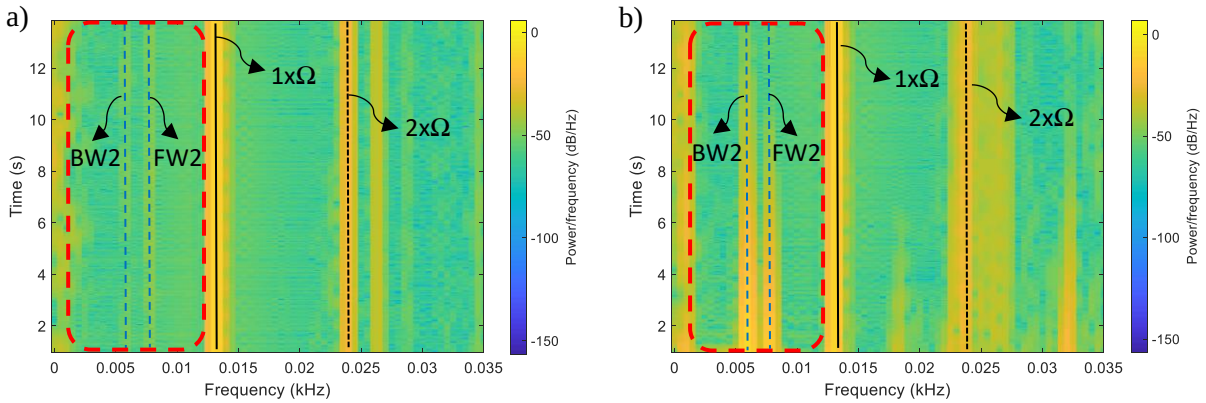

Figure 12: Steady-state test spectrogram (air speed 2.2 m/sec): a) without impulse, b) with impulse

4.2.3 Numerical and experimental correlation

Experimentally and numerically determined natural frequencies of the BWRR are compared in Table 4 for selected rotating conditions. The rotor and wind speeds during this experiment were found to be 824 rpm ≈ 13.73 Hz and 2.5 m/sec, respectively, and the numerical modal analysis was executed for the same set of operational parameters.

Table 4: Experimental and numerical lateral mode comparison of the BWRR (824 rpm, 2.5 m/sec)

Lateral Mode #	Numerical Natural Freq. [Hz]	Experimental Natural Freq. [Hz]	Error %	Mode Type
1	0.57	0.87	34.0	Lateral BW
2	0.94	1.00	5.8	Lateral FW
3	6.06	5.93	2.1	Lateral BW
4	8.78	7.80	12.5	Lateral FW

From this table, the errors between the numerically and experimentally determined natural frequencies can be thought to be satisfactory in all cases except for the significant discrepancy in mode 1 (BW1). Ignoring aerodynamic forces and moments in the dynamic modelling is thought to be one of the reasons of this discrepancy. The results of the numerical BWRR modal analysis are also summarised in Figure 13 for all four lateral modes of interest, where lateral backward and forward whirling mode shapes are clearly seen.

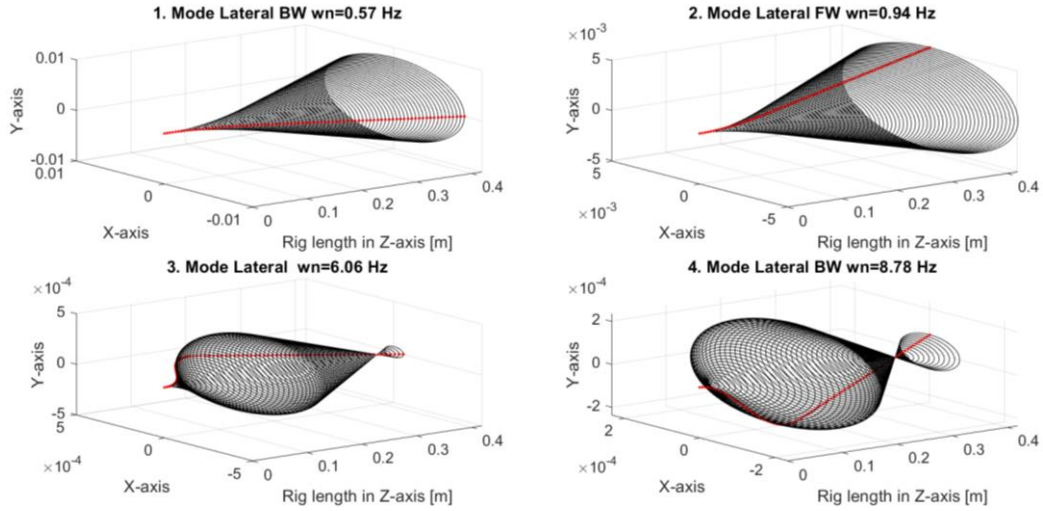

Figure 13: Computed mode shapes of the BWRR at 824 rpm

For these modes, experimentally and numerically obtained natural frequencies are summarised with respect to the wind tunnel's fan voltage in Figure 14. When comparing the experimental and numerical values, it can be seen that the lateral backward and forward modes have similar rate of decrease and increase, respectively. Furthermore, the identified rotor speed matches the 2nd lateral mode family between 6 and 8 Hz at the 7V fan control input. This result is consistent with that presented in Figure 9 where the strong resonance occurrence is observed during the run-up test in the close proximity of the same frequency values. Theoretically, BW1 and FW1 may also experience resonance at around 1V. However, in practice, the propeller does not rotate in relatively weak air stream produced by the fans at 1V. Therefore, no resonance is observed in connection with the 1st lateral mode family in the current configuration. Finally, both sets of results indicate their satisfactory mutual correlation as well as further potential in modelling improvement.

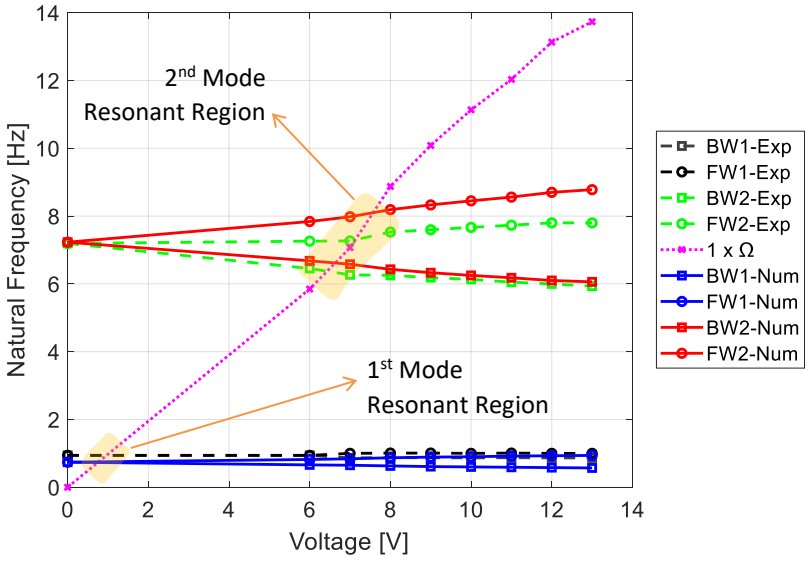

Figure 14: Numerical and experimental natural frequency map

5 Discussion

Numerical and experimental modal analysis as well as initial comparison of the determined natural frequencies is the main focus of this study. On the modelling side, a new 3D beam element-based model of the BWRR was developed using the finite element method, which included the effects of gyroscopic and gravity forces. On the experimental side, a simple yet robust process for natural frequency and modal damping identification and in-operation tracking was demonstrated. The proposed procedure involves combined application of the cepstrum, peak-finding and filtering tools followed by the use of the modified logarithmic decrement method for natural frequency and modal damping identification.

In the first stage, the non-rotating test rig is characterized with EMA and numerical modal analysis in the linear response regime. First four lateral modes are successfully captured with both experimental and numerical modal analysis. It should be noted that EMA was only carried out in the lateral directions, therefore numerically identified torsional modes could not be detected. In the second stage, vibrational behaviour of the rotating test rig is studied in operation across changing air stream speed with experimental and numerical vibration analyses. Lateral BW and FW modes and harmonics related to the propeller rotation were successfully detected with the experiments in the run-up and steady state vibration tests. A good initial correlation between the experimental vibration analysis and numerical computations was found for the non-rotating and rotating modal behaviour of the 1st and 2nd lateral mode families in terms of their natural frequencies. Assuming low damping, natural frequency estimation with peak-finding and modal damping estimation with logarithmic decrement method present particularly useful results for the 2nd lateral mode family. However, the quality of the 1st lateral mode family identification is found to be insufficient because the 1st BW and FW lateral modes are very close to each other, requiring the use of enhanced test and identification procedure in future. Among these required improvements, more focused impulse excitation and longer data acquisition periods for higher frequency resolution are needed.

Throughout experiments, there were various nonlinear effects observed such as free-play nonlinearity due to the blade and rotor-hub joint imperfections and misalignments as well as geometric nonlinearity during the resonant rig response. These nonlinearities affect the correlation between the numerical and experimental results. During the non-rotating modal analysis, only the first two lateral mode families could be detected successfully using experimental methods because acceleration response and force input locations did not allow detection of the higher modes properly. For identification of these modes accurately, full scale experimental modal analysis is needed, in which FRFs should be collected from a sufficient number of measurement locations. In the rotating case modal studies, the rotor frequency higher harmonics were observed because of the unwanted distortion in the uniformness of the air stream speed in the wind tunnel as well as due to other mechanical and aerodynamic imperfections in the rig. For example, air speed can fluctuate during the operation leading to the fluctuating aerodynamic forcing, which can lead to other unbalanced loading to be experienced by the rig during its operation. This makes the harmonics tracking and narrow band detection for subsequent filtering challenging. Furthermore, decoupling of the test rig from the vertical wind tunnel is necessary for eliminating the possible harmonics in the BWRR induced by the wind tunnel's fans. Finally, to achieve a better focused modal excitation, an impact device with suitably soft tip can be employed for achieving improved impact rig excitation during the wind tunnel operation.

Numerical modelling has its own limitations in term of achieving representative simulations of the real experimental environment in the vertical wind tunnel. For example, the current dynamic model does not include aerodynamic forces and moments and their resulting aeroelastic effect on the rotor. Therefore, aeromechanical analyses including aeroelastic stability assessment were not provided in this study. For further improvement and accurate modelling, aerodynamic forces and moments on the rotor, as well as the corresponding experimental data, should be included in the future dynamic modelling to achieve better validation.

6 Conclusion

A novel whirl flutter test rig called the Bristol Whirling Rotor Rig (BWRR) was developed and presented. The dynamics of BWRR was investigated in both stationary and free-rotating (windmilling) conditions, with the latter operated within a vertical wind tunnel. The results of initial experimental studies on the BWRR combining impact hammer tests, run-up and steady-state vibration tests were presented and discussed in this paper. For the non-spinning configuration, the first and second lateral mode families of the BWRR were clearly detected in the identified FRFs. Likewise, the backward and forward whirling modes as well as the rotational frequencies with their harmonics were observed in both run-up and steady-state vibration tests, when the rig was operated in the wind tunnel. The initial version of the modal parameter monitoring procedure was also proposed and evaluated. Here, the natural frequencies and modal damping were proposed to be identified with the peak-finding and logarithmic decrement methods, respectively. The modal parameter estimation procedure was found to be reliable and automatable for the second lateral mode family while it became insufficient for the first lateral mode family because of the low frequency resolution, low frequency values and close peak separation. For the numerical analyses, a new beam element-based dynamic model of the BWRR, which includes the gravity and gyroscopic forces, was created using the finite element method. The experimental and computed natural frequencies were compared and sources of errors discussed. Overall, there was a relatively higher agreement in the second mode family than in the first one.

In the future, an enhanced OMA procedure for mode tracking and whirl flutter identification will be developed. In particular, the stochastic subspace identification approach and other automatable techniques will be considered for use in online mode tracking. The dynamic model will be updated by incorporating aerodynamic moments and forces for conducting aeroelastic stability analyses. These studies will contribute to assessing the feasibility of an early warning whirl flutter detection and online rotor monitoring system in large scale test campaigns.

Acknowledgements

This research is part of MENTOR (Methods and Experiments for Novel Rotorcraft) project, which is funded by the Engineering and Physical Sciences Research Council (EPSRC) under Grant No. EP/S010378/1.

References

[1] W. H. Reed, “Propeller-Rotor whirl flutter,” *J. Sound Vib.*, vol. 4.3, pp. 526–544, 1966, doi: 526IN31531-530544.

[2] R. L. Bielawa, *Rotary wing structural dynamics and aeroelasticity*. American Institute of Aeronautics and Astronautics, 2006.

[3] J. Cecrdle, *Whirl Flutter of Turboprop Aircraft Structures*. Elsevier, 2015.

[4] W. Johnson, “Dynamics of tilting proprotor aircraft in cruise flight,” 1974.

[5] C. Mair, D. Rezgui, and B. Titurus, “Nonlinear stability analysis of whirl flutter in a rotor-nacelle system,” *Nonlinear Dyn.*, vol. 94, no. 3, pp. 2013–2032, 2018, doi: 10.1007/s11071-018-4472-y.

[6] C. W. Acree, R. J. Peyran, and W. Johnson, “Improving Tiltrotor Whirl-Mode Stability with Rotor Design Variations,” p. 14, 2000.

[7] C. W. Acree, R. J. Peyran, and W. Johnson, “Rotor design for whirl flutter: An examination of options for improving tiltrotor aeroelastic stability margins,” *Annu. Forum Proc. - Am. Helicopter Soc.*, vol. 1, pp. 997–1012, 1999.

[8] C. W. Acree, “Rotor Design Options for Improving V-22 Whirl-Mode Stability,” *Society*, 2001.

[9] E. L. Hathaway and F. Gandhi, "Design optimization for improved tiltrotor whirl flutter stability," *J. Am. Helicopter Soc.*, vol. 52, no. 2, pp. 79–89, 2007, doi: 10.4050/JAHS.52.79.

[10] J. Arnold and S. Waitz, "Using multibody dynamics for the stability assessment of a new rotor test rig," *43rd Eur. Rotorcr. Forum, ERF 2017*, vol. 2, pp. 1238–1247, 2017.

[11] C. W. Acree and A. L. Sheikman, "Development and initial testing of the tiltrotor test rig," *Annu. Forum Proc. - AHS Int.*, vol. 2018-May, 2018.

[12] A. Datta, F. Tsai, and J. Sutherland-Foggio, "Design of a new tiltrotor test facility at the university of maryland," *AIAA Scitech 2019 Forum*, no. January, pp. 1–19, 2019, doi: 10.2514/6.2019-2136.

[13] A. R. Kreshock, H. Kang, H. Yeo, and C. W. Acree, "Development of a new aeroelastic tiltrotor wind tunnel testbed," *AIAA Scitech 2019 Forum*, no. January, 2019, doi: 10.2514/6.2019-2133.

[14] G. Gibertini, P. Milano, and C. Bovisa, "Gibertini G , Auteri F , Campanardi G , et al. Wind-tunnel tests of a tilt-rotor aircraft," *Aeronaut. J.*, vol. 115, no. 1167, pp. 315–322, 2011.

[15] C. W. Acree, A. L. Sheikman, and T. R. Norman, "High-speed wind tunnel tests of a full-scale proprotor on the tiltrotor test rig," *Vert. Flight Soc. - Forum 75 Futur. Vert. Flight - Proc. 75th Annu. Forum Technol. Disp.*, vol. 1, pp. 1–19, 2019.

[16] W. R. Krüger, "Multibody analysis of whirl flutter stability on a tiltrotor wind tunnel model," *Proc. Inst. Mech. Eng. Part K J. Multi-body Dyn.*, vol. 230, no. 2, pp. 121–133, Jun. 2016, doi: 10.1177/1464419315582128.

[17] J. Cecrdle, J. Malecek, O. Vich, and P. Malinek, "Development and wind tunnel test of W-WING whirl flutter aeroelastic demonstrator," *57th AIAA/ASCE/AHS/ASC Struct. Struct. Dyn. Mater. Conf.*, no. January, 2016, doi: 10.2514/6.2016-1961.

[18] J. Cecrdle, O. Vich, and P. Malinek, "Wind tunnel test of a whirl flutter aeroelastic demonstrator," *Proc. Inst. Mech. Eng. Part G J. Aerosp. Eng.*, vol. 233, no. 3, pp. 969–977, 2019, doi: 10.1177/0954410017744237.

[19] M. Böswald, Y. Govers, G. Jelicic, and R. Buchbach, "Online monitoring of flutter stability during wind tunnel testing of an elastic wing with pylon and engine nacelle within the HMAE1 project," in *International Forum on Aeroelasticity and Structural Dynamics 2019, IFASD 2019*, 2019, no. June, pp. 1–14.

[20] G. Coppotelli, F. Di Giandomenico, P. Marzocca, and M. Marino, "Real-time system identification for fixed-wing aircraft," *AIAA Scitech 2019 Forum*, no. January, pp. 1–13, 2019, doi: 10.2514/6.2019-1533.

[21] E. Di Lorenzo *et al.*, "Structural dynamics assessment on a full-electric aircraft: Ground vibration testing and in-flight measurements," in *International Forum on Aeroelasticity and Structural Dynamics 2019, IFASD 2019*, 2019, no. June, pp. 1–17.

[22] W. H. Reed III and R. M. Bennett, "Propeller Whirl Flutter Considerations for V/STOL Aircraft," *CAL-TRECOM Symp.*, 1963.

[23] M. I. Friswell, J. E. T. Penny, S. D. Garvey, and A. W. Lees, *Dynamics of Rotating Machines*. Cambridge: Cambridge University Press, 2010.

[24] R. Brincker and C. Ventura, *Introduction to operational modal analysis*. John Wiley & Sons, 2015.

[25] R. B. Randall, "A history of cepstrum analysis and its application to mechanical problems," *Mech. Syst. Signal Process.*, vol. 97, pp. 3–19, 2017, doi: 10.1016/j.ymssp.2016.12.026.

[26] D. J. Inman, *Engineering vibration*, vol. 3. Prentice Hall New Jersey, 2008.